Available online at www.sciencedirect.com
SCIENCE DIRECT
Journal of Power Sources 157 (2006) 875–885
JOURNAL OF POWER SOURCES
www.elsevier.com/locate/jpowsour

Prediction of anode performances of direct methanol fuel cells with different flow-field design using computational simulation

Min-soo Hyun [a,b], Sang-Kyung Kim [a], Doohwan Jung [a,*], Byungrock Lee [a], Donghyun Peck [a], Taejin Kim [a], Yonggun Shul [b]

[a] *Advanced Fuel Cell Research Center, Korea Institute of Energy Research, 71-2 Jang-dong, Yuseong-gu, Daejeon 305-343, Republic of Korea*
[b] *Department of Chemical Engineering, Yonsei University, Seoul 120-749, Republic of Korea*

Received 6 October 2005; received in revised form 2 February 2006; accepted 6 February 2006
Available online 18 April 2006

Abstract

Three-dimensional computational simulation was employed to illustrate the performance characteristics according to the flow-field design by solving the physics in the flow field and the diffusion layer and by calculating the electrochemical reaction at the catalyst layer. The pressure loss and the concentration distribution in the anode were analyzed for four types of flow field, parallel, serpentine, parallel serpentine and zigzag type. Also the anode current density distribution was predicted at the various overpotentials. The cell performance was proportional to the pressure drop for all the flow-field types. Zigzag type showed the best performance which has a good resistance against the fuel concentration polarization and the next was serpentine.

Keywords: Direct methanol fuel cells; Flow field; Current density distribution; Computational simulation; Anode overpotential

1. Introduction

Because of the convenience of fuel storage and the compactness, direct methanol fuel cell (DMFC) is the most remarkable type for potable applications among all kinds of fuel cells [1,2]. DMFC is similar to proton exchange membrane fuel cell (PEMFC) in using polymer membrane as electrolyte but different in using liquid methanol as fuel. The fact that DMFC uses liquid fuel offers an advantage in fuel storage but brings about other problems. One is methanol crossover to the cathode side. Methanol crossover is mainly occurred by diffusion and by electro-osmotic drag. Methanol crossover makes a mixed potential at the cathode and therefore it decreases the cell performance. Several earlier researchers have investigated about methanol permeation to find out the exact mechanism and to reduce methanol crossover [3–8]. The other problem is two-phase flow. Carbon dioxide produced by methanol oxidation is gaseous phase although methanol–water mixture is liquid phase. Therefore, it causes a big pressure loss in the flow fields and also makes gas blocks which keep liquid fuel from diffusing into the catalyst surface [9–12]. In addition, it is difficult to make uniform concentration because the diffusivity of methanol is smaller than hydrogen gas. DMFC is greatly related not only to a low catalytic activity of methanol electrooxidation but to mass transfer problems. Anodic, cathodic and overall reactions of DMFC as follows:

$$\text{Anode}: CH_3OH + H_2O \rightarrow CO_2 + 6H^+ + 6e^- \quad (1)$$

$$\text{Cathode}: \tfrac{3}{2}O_2 + 6H^+ + 6e^- \rightarrow 3H_2O \quad (2)$$

$$\text{Overall}: CH_3OH + \tfrac{3}{2}O_2 \rightarrow CO_2 + 2H_2O \quad (3)$$

The polarization of fuel cell generally consists of activation, ohmic and concentration polarization. The shape of flow field affects the increase of the concentration overpotential due to concentration polarization which is derived from the lack of fuel. The effect of the concentration polarization is stronger at the anode side than at the cathode side because of the slow mass transfer of the liquid fuel. At the cathode side it is more important to remove water.

Kulikovsky et al. [13] accomplished two-dimensional modeling based on mass and current conservation and found out

* Corresponding author. Tel.: +82 42 860 3577; fax: +82 42 860 3309.
E-mail address: doohwan@kier.re.kr (D. Jung).

0378-7753/$ – see front matter © 2006 Elsevier B.V. All rights reserved.
doi:10.1016/j.jpowsour.2006.02.023

Nomenclature

c	molar concentration (mol m^{-3} or M)
c^{MeOH}	molar concentration of methanol (mol m^{-3} or M)
c_0^{MeOH}	initial molar concentration of methanol (mol m^{-3} or M)
$c_{\mathrm{threshold}}^{\mathrm{MeOH}}$	molar concentration of methanol at threshold point (mol m^3 or M)
D	diffusion coefficient (m^2 s^{-1})
$D_{\mathrm{MeOH,w}}$	diffusion coefficient of methanol in water (m^2 s^{-1})
$D_{\mathrm{MeOH,w}}^{\mathrm{eff}}$	effective diffusion coefficient of methanol in water (m^2 s^{-1})
F	Faraday constant (96,487)
$\mathbf{F}$	volume force
I	current density (A m^{-2})
I_0^{MeOH}	exchange current density of methanol oxidation (A m^{-2})
$I_{0,\mathrm{ref}}^{\mathrm{MeOH}}$	exchange current density of methanol oxidation at reference point (A m^{-2})
k	permeability (m^2)
$\mathbf{n}$	a normal vector to the boundary
$\mathbf{N}_{\mathrm{reaction}}$	flux derived by reaction (mol m^{-2} s^{-1})
p	pressure (Pa)
$p_{\mathrm{interface}}$	pressure at the interface between channel and backing layer (Pa)
R	gas constant (8.314 J mol^{-1} K^{-1})
t	time (s)
T	temperature (K)
$\mathbf{u}$	velocity vector (m s^{-1})
u_0	initial line velocity (m s^{-1})

Greek letters

α_{a}	anodic transfer coefficient
ε	porosity
η_{a}	anodic overpotential (V)
μ	viscosity (kg m^{-1} s^{-1})
ρ	density (kg m^{-3})

that the transport of methanol was determined by the pressure gradient and that the creation of 'Shaded' zone was dependent on the hydraulic permeability of the backing layer. Wang and Wang [14] simulated two-phase flow in liquid-feed DMFC by the two-dimensional model which included the calculation of the current density distribution and the methanol crossover flux and the prediction of the unit cell performance. Scott and Argyropoulos [15] studied one-dimensional model of DMFC focused on electrocatalysis to predict anode polarization behavior. Dohle and Wippermann [16] investigated the anode overpotential, the cathode overpotential and the methanol permeation in order to experimentally obtain an empirical equation. Their model described the current density characteristics and the methanol permeation. Although the above models were mainly mathematical approaches about the electrochemical reaction and the mass transfer, they did not include the effect of flow fields. On the researches about the flow-field pattern, Arico et al. [17] investigated the features of the serpentine and interdigitated flow-field type for DMFC. According to their experiments, the interdigitated type significantly enhanced the mass transport and hence showed the higher maximum power outputs compared to the classical serpentine geometry. Tüber et al. [18] measured the performance of PEMFC and DMFC for serpentine, parallel and fractal type of flow field as the flow-field design and the serpentine type showed the best result. They speculated that the serpentine channel forces the products out of the cell by its higher pressure drop and that the parallel and fractal designs can suffer from the blocked channels by inhomogeneous flow distribution.

In this work three-dimensional computational simulation was used in order to illustrate the causes of performance difference according to the flow-filed design. Parallel, serpentine, parallel serpentine and zigzag shapes were simulated and estimated for the flow field of the anode by comparing the concentration distribution and the current density distribution at the various overpotentials.

2. Experimental

FEMLAB, a commercial program, is used in this work.

2.1. Assumptions

1. The DMFC system is steady state.
2. Gravity is ignored.
3. The system is isothermal.
4. Two-phase flow due to carbon dioxide is ignored.
5. Vaporization and crossover of the anode fuel are ignored.
6. The flow is laminar and incompressible.
7. Fuel consumption does not affect Navier–Stokes momentum balance in the fuel channel.
8. Thickness of the catalyst layer is zero.
9. Fuel concentration change due to water consumption is ignored.

2.2. Geometry

Fig. 1 shows the components of DMFC. Flow-field plate plays the part of the fuel flow field and of the current collector from membrane electrode assembly (MEA). Fuel flows through the fuel channels and diffuses into the backing layer. The backing layer supports the catalyst layer and controls the fuel diffusion into the catalyst layer. Electrochemical oxidation and reduction occurred at the catalyst layer and membrane plays a part in the proton conduction. The simulated part in this study is the anode side, the inside of the red box in Fig. 1. An overview of the geometry is shown in Fig. 2.

Four types of the flow field which is parallel, serpentine, parallel serpentine and zigzag were used for the simulation. In all cases, fuel input and fuel output are located diagonal to each other and the electrode area is about 2.25 cm^2. Height and width of the channel are fixed as 1 mm. Fuel flows according to the flow fields are described in Fig. 3 and the geometrical specifications are shown in Table 1.

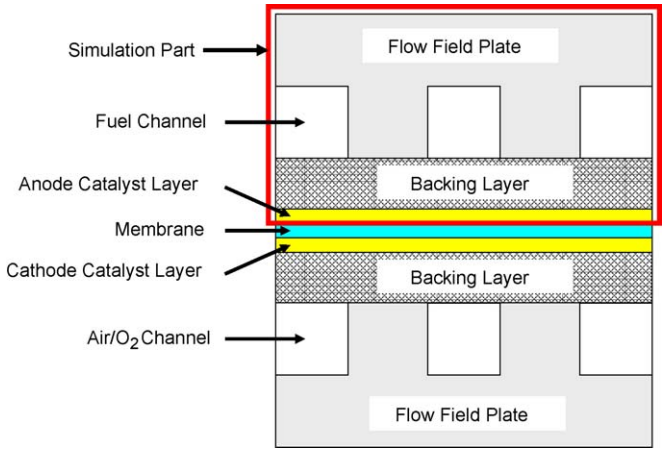

Fig. 1. Cross-sectional view of a DMFC and the simulation part.

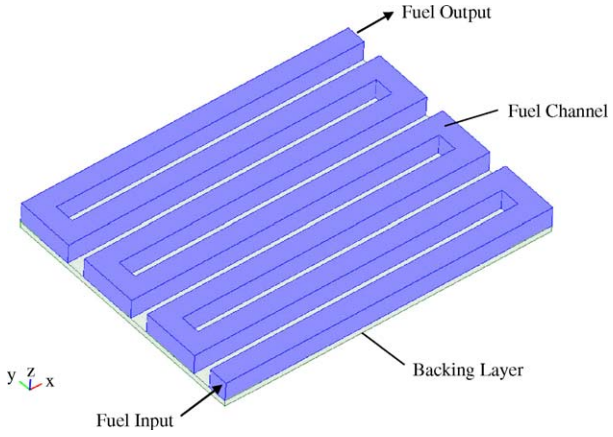

Fig. 2. An overview of the geometry (serpentine type).

Table 1
Specifications of the flow fields

	Electrode area (cm^2)	Width × length (cm^2)	Channel area (cm^2)	Rib area (cm^2)	Rib area ratio
Parallel	2.25	1.5 × 1.5	1.41	0.84	0.373
Serpentine	2.21	1.7 × 1.3	1.25	0.96	0.434
Parallel serpentine	2.255	2.05 × 1.1	1.32	0.935	0.415
Zigzag	2.2575	1.5 × 1.55	1.3875	0.87	0.385

2.3. Governing equations

In the flow-field channel, Navier–Stokes equations (Eq. (4)) were employed to calculate velocity and pressure. The momentum balance and the continuity equation are as follows:

$$\rho\frac{\partial \mathbf{u}}{\partial t} - \nabla \cdot \mu(\nabla \mathbf{u} + (\nabla \mathbf{u})^{\mathrm{T}}) + \rho(\mathbf{u} \cdot \nabla)\mathbf{u} + \nabla P = \mathbf{F} \tag{4}$$

$$\nabla \cdot \mathbf{u} = 0 \tag{5}$$

where $\mathbf{F}$ denotes the volume force term such as gravity force.

On the other hand, the momentum balance in the porous backing layer can be described by Darcy's law,

$$\mathbf{u} = -\frac{k}{\mu}\nabla P \tag{6}$$

The convective velocity is determined by pressure gradient because the permeability and the viscosity are constant. Pressure gradient can be derived from Navier–Stokes equations because the flow-field channel and the backing layer are contacted each other.

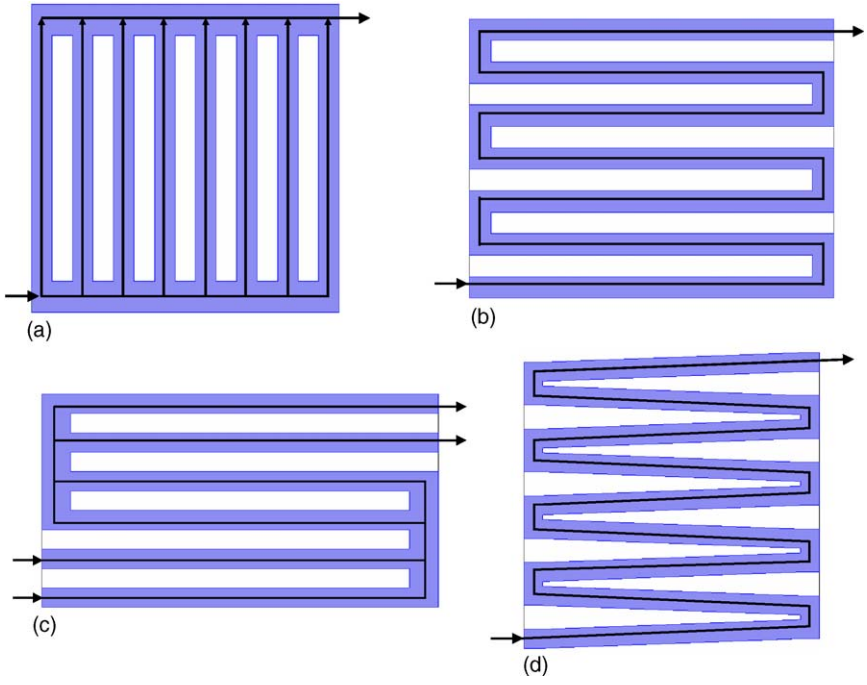

Fig. 3. Fuel flows according to the flow-field type: (a) parallel, (b) serpentine, (c) parallel serpentine and (d) zigzag.

Table 2
Physical and chemical properties

Parameter	Value	Reference
Anodic transfer coefficient, α_a	0.239	[14]
Reference exchange current density of methanol oxidation at 80 °C, $I_{0,ref}^{MeOH}$ (A m^{-2})	94.25	[14]
Cell temperature, T (K)	353	
Channel height, h (m)	0.001	
Channel width, w (m)	0.001	
Density of 1 M methanol, ρ (kg m^{-3})	980	Measured
Diffusion coefficient of methanol in water, D_{MeOH} (m^2 s^{-1})	$10^{-5.4163-999.778/T}$	[14]
Input methanol concentration, c_0^{MeOH} (mol m^{-3})	1000	
Input velocity of fuel, v (m^3 s^{-1})	1.5×10^{-8}	
Permeability of backing layer, k (m^2)	1×10^{-11}	Assumed
Porosity of backing layer, ε	0.77	Assumed
Thickness of backing layer, l (m)	0.0003	Assumed
Viscosity of methanol–water mixture, μ (kg m^{-1} s^{-1})	$0.458509-5.304741\times10^{-3}T+2.31231\times10^{-5}T^2-4.49161\times10^{-8}T^3+3.27681\times10^{-11}T^4$	[19]

The convection and diffusion equation is,

$$\frac{\partial c}{\partial t} = \nabla\cdot(D\nabla c - c\mathbf{u}) \tag{7}$$

The expression within the parenthesis represents the flux, where the first term describes the transport by diffusion and the second represents the convective flux. The velocity of the convective flux was obtained by Navier–Stokes equations or Darcy's equation.

The bottom of the backing layer is regarded as the catalyst layer. In the catalysts layer only the electrochemical kinetics are considered because the thickness of the catalyst layer is assumed as zero. In this work, Tafel kinetic equation of methanol oxidation was used which was proposed by Wang and Wang [14]. According to Tafel equation, methanol oxidation is a zero-order reaction when the methanol concentration is higher than 0.1 M. But under the threshold value, 0.1 M, the methanol oxidation is considered as a first-order reaction and the exchange current density decreases rapidly (Table 2).

$$I = I_0^{MeOH}\exp\left(\frac{\alpha_a F}{RT}\eta_a\right) \tag{8}$$

$$I_0^{MeOH} = I_{0,ref}^{MeOH}\left(\frac{c^{MeOH}}{c_{threshold}^{MeOH}}\right)^n \tag{9}$$

$$n = \begin{cases} 0; & (c^{MeOH} \geq c_{threshold}^{MeOH}) \\ 1; & (c^{MeOH} < c_{threshold}^{MeOH}) \end{cases} \qquad c_{threshold}^{MeOH} = 0.1\,\mathrm{M} \tag{10}$$

2.4. Boundary conditions and parameters

2.4.1. Navier–Stokes equations

At wall,

$$\mathbf{u} = 0 \tag{11}$$

At the entrance of fuel input,

$$\mathbf{u}\cdot\mathbf{n} = u_0 \tag{12}$$

where u_0 is the line velocity of fuel.
At the exit of fuel output,

$$p = 0 \tag{13}$$

2.4.2. Darcy's law

At wall,

$$-\frac{k}{\mu}\nabla p\cdot\mathbf{n} = 0 \tag{14}$$

At the interface between the flow-field channel and the backing layer,

$$p = p_{interface} \tag{15}$$

where $p_{interface}$ is derived from Navier–Stokes equations.

2.4.3. Convection and diffusion equation

The diffusion coefficient in the porous backing layer is corrected with the porosity of the backing layer by Bruggemann's correction,

$$D_{MeOH,w}^{eff} = D_{MeOH,w}\times\varepsilon^{1.5} \tag{16}$$

The effective diffusion coefficient was used in the backing layer domain and the bulk diffusion coefficient was used in the fuel channel domain.

The velocity from Navier–Stokes equations was used in the channel domain and the convection velocity from Darcy's law was used in the backing layer.

At wall,

$$(D\nabla c - c\mathbf{u})\cdot\mathbf{n} = 0 \tag{17}$$

At the entrance of the fuel input,

$$c = c_0^{MeOH} \tag{18}$$

where c_0^{MeOH} is the initial methanol concentration.
At the exit of the fuel output,

$$\mathbf{n}\cdot(D_{MeOH,w}\nabla c) = 0 \tag{19}$$

At the bottom of the backing layer,

$$(D_{MeOH,w}^{eff}\nabla c - c\mathbf{u})\cdot\mathbf{n} = \mathbf{N}_{reaction} \tag{20}$$

where $\mathbf{N}_{reaction}$ is the methanol flux which is obtained from the methanol oxidation kinetics.

2.4.4. Kinetic equation of methanol oxidation

The exchange current density (9) can be rewritten as follows:

$$I_0^{\mathrm{MeOH}} = I_{0,\mathrm{ref}}^{\mathrm{MeOH}} + \frac{(I_{0,\mathrm{ref}}^{\mathrm{MeOH}}/c_{\mathrm{threshold}}^{\mathrm{MeOH}})(c^{\mathrm{MeOH}} - c_{\mathrm{threshold}}^{\mathrm{MeOH}}) - |(I_{0,\mathrm{ref}}^{\mathrm{MeOH}}/c_{\mathrm{threshold}}^{\mathrm{MeOH}})(c^{\mathrm{MeOH}} - c_{\mathrm{threshold}}^{\mathrm{MeOH}})|}{2} \tag{21}$$

Therefore, Tafel kinetic equation (Eq. (8)) can be rewritten as follows:

$$I = \left(I_{0,\mathrm{ref}}^{\mathrm{MeOH}} + \frac{(I_{0,\mathrm{ref}}^{\mathrm{MeOH}}/c_{\mathrm{threshold}}^{\mathrm{MeOH}})(c^{\mathrm{MeOH}} - c_{\mathrm{threshold}}^{\mathrm{MeOH}}) - |(I_{0,\mathrm{ref}}^{\mathrm{MeOH}}/c_{\mathrm{threshold}}^{\mathrm{MeOH}})(c^{\mathrm{MeOH}} - c_{\mathrm{threshold}}^{\mathrm{MeOH}})|}{2} \right) \exp\left(\frac{\alpha_{\mathrm{a}} F}{RT} \eta_{\mathrm{a}} \right) \tag{22}$$

and the methanol flux is

$$\mathbf{N}_{\mathrm{reaction}} = -\frac{1}{6F} \left(I_{0,\mathrm{ref}}^{\mathrm{MeOH}} + \frac{(I_{0,\mathrm{ref}}^{\mathrm{MeOH}}/c_{\mathrm{threshold}}^{\mathrm{MeOH}})(c^{\mathrm{MeOH}} - c_{\mathrm{threshold}}^{\mathrm{MeOH}}) - |(I_{0,\mathrm{ref}}^{\mathrm{MeOH}}/c_{\mathrm{threshold}}^{\mathrm{MeOH}})(c^{\mathrm{MeOH}} - c_{\mathrm{threshold}}^{\mathrm{MeOH}})|}{2} \right) \exp\left(\frac{\alpha_{\mathrm{a}} F}{RT} \eta_{\mathrm{a}} \right) \tag{23}$$

3. Result and discussions

The calculated methanol concentration distribution in the overall geometry of the serpentine type is shown in Fig. 4 when the overpotential of 0.45 V is imposed to the electrode. The concentration difference between the flow field and the catalyst layer is big while the difference between fuel input and output in the flow fields is not big. Particularly, concentration at rib areas of the catalyst layer which contact with bipolar plate is very low because fuel cannot contact with the backing layer directly. Methanol concentration at the catalyst layer is much lower than in the flow fields and there is also a wide difference of methanol concentration among the positions on the catalyst layer.

When the overpotential of 0.3 V is imposed, the methanol concentration distributions at the catalyst layers are shown in Fig. 5. The minimum methanol concentrations are higher than 100 mol m^{-3}, the threshold value, for all the flow-field types, although low concentrations which are expressed in blue in Fig. 5 are shown at ribs for parallel and parallel serpentine type. Therefore, there are no current deviations within the all catalyst layers and the calculated current densities for all the flow-field types are 995 A m^{-2} equally.

Fig. 6 shows the methanol concentration distributions when the overpotential of 0.4 V is imposed. The zigzag type shows the highest average concentration and the parallel type is the lowest. Comparing Fig. 5, overall methanol concentration decreased greatly due to the increment of oxidation kinetics. Methanol concentration of parallel type reaches to the threshold value on the whole areas of the catalyst layer. Fig. 7 shows the current density distributions when the overpotential of 0.4 V is imposed. Dead zone is observed at the ribs of the parallel and parallel serpentine types partially although the serpentine and zigzag did not yet fall into the concentration polarization.

In the case of 0.45 V overpotential (Figs. 8 and 9), most sections of the parallel and the parallel serpentine reach to the threshold. The serpentine type starts to fall into the concentration

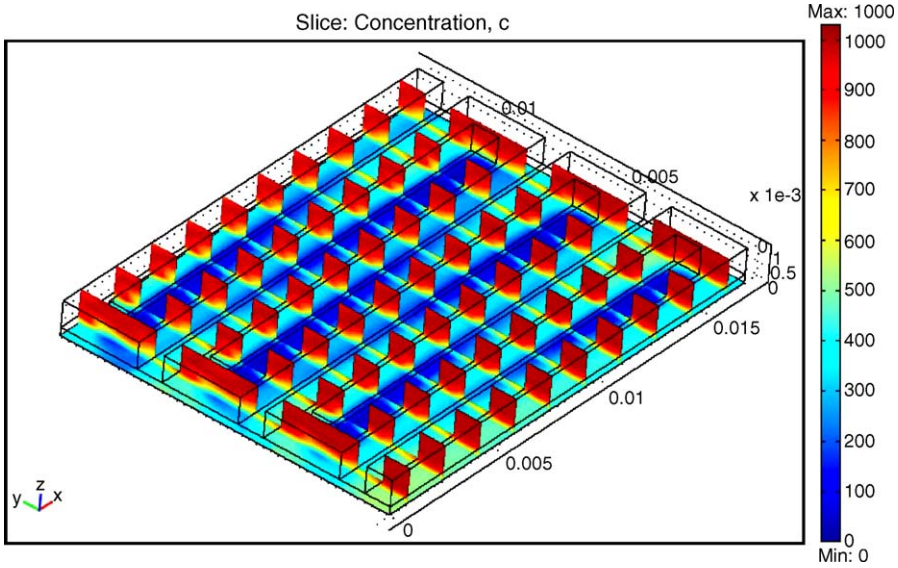

Fig. 4. The distribution of the calculated methanol concentration for the serpentine type when the overpotential of 0.45 V is imposed (unit: mol m^{-3}).

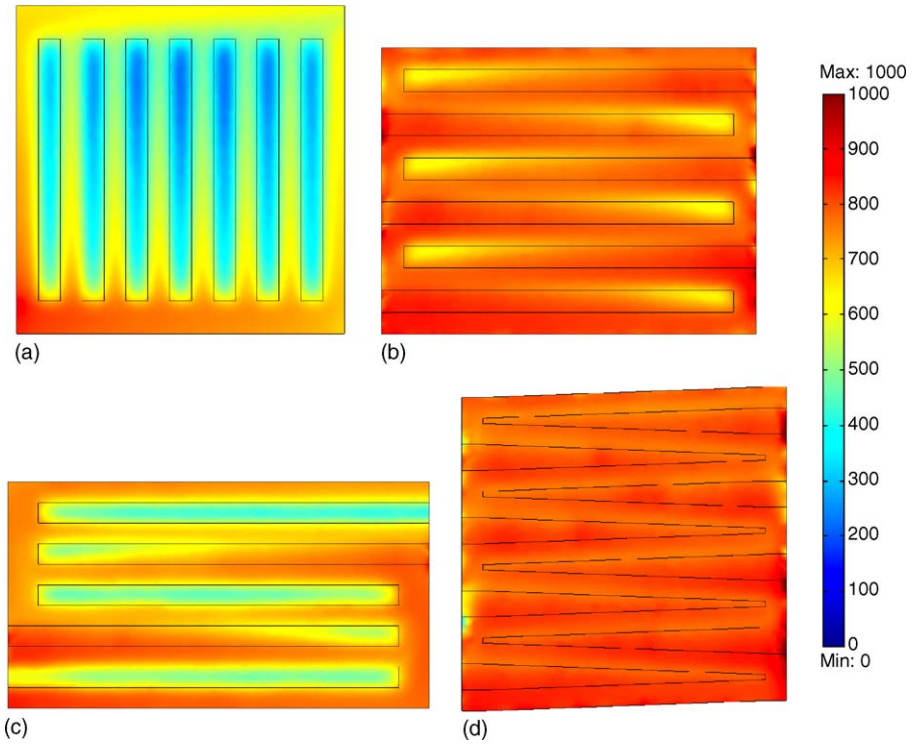

Fig. 5. Concentration distributions at the electrode surface when the overpotential of 0.3 V is imposed. Average concentrations on the catalyst layer: (a) 525 mol m^{-3} for parallel, (b) 780 mol m^{-3} for serpentine, (c) 676 mol m^{-3} for parallel serpentine and (d) 803 mol m^{-3} for zigzag.

polarization although zigzag type is still keeping the theoretical current density without concentration polarization. When 0.5 V overpotential is imposed (Figs. 10 and 11), a significant lack of methanol appeared in all types of the flow field and also the difference in the current densities increased within each catalyst layer. The concentration polarization generates easily at ribs and this area acts as 'dead zone' at which current density decreases rapidly. In case of the zigzag and the serpentine types, relatively

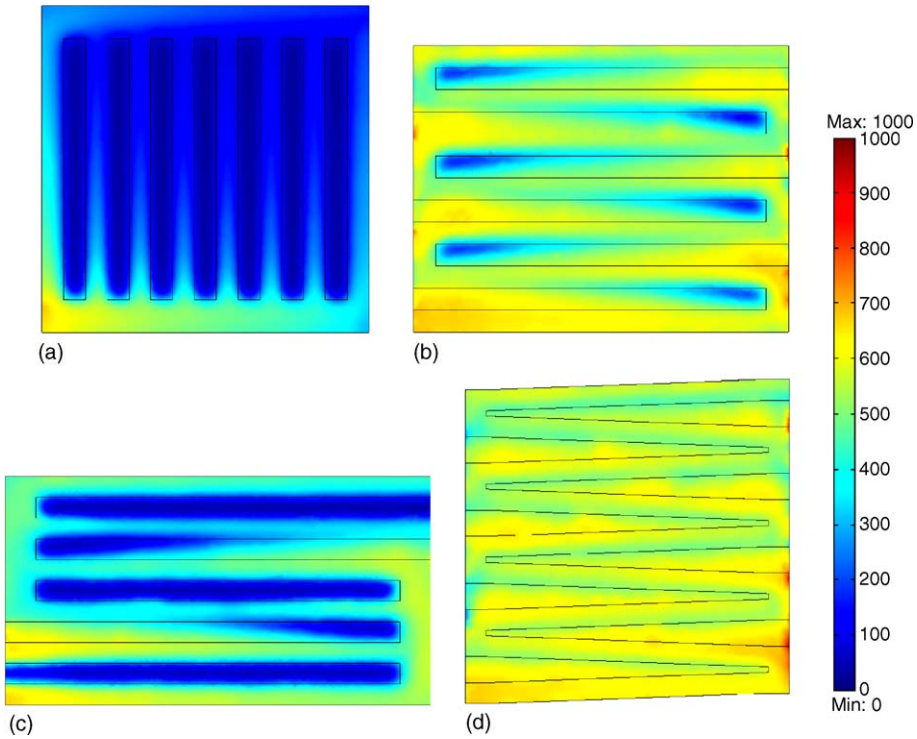

Fig. 6. Concentration distributions at the electrode surface when the overpotential of 0.4 V is imposed. Average concentrations on the catalyst layer: (a) 178 mol m^{-3} for parallel, (b) 517 mol m^{-3} for serpentine, (c) 338 mol m^{-3} for parallel serpentine and (d) 570 mol m^{-3} for zigzag.

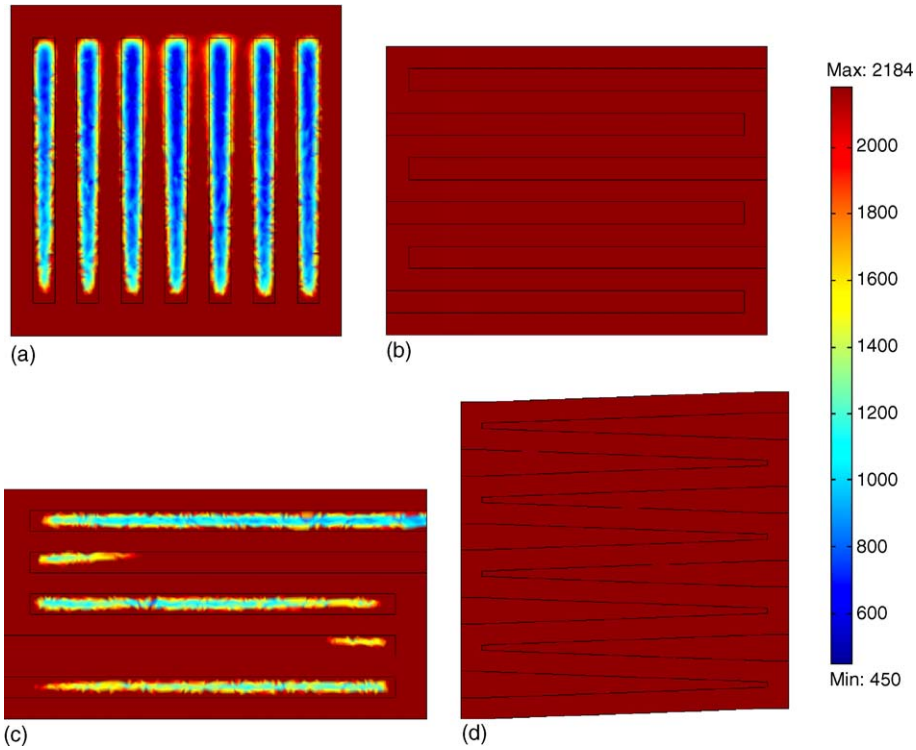

Fig. 7. Current distributions at the electrode surface when the overpotential of 0.4 V is imposed. Average current densities on the catalyst layer: (a) 1827 A m^{-2} for parallel, (b) 2184 A m^{-2} for serpentine, (c) 2086 A m^{-2} for parallel serpentine and (d) 2184 A m^{-2} for zigzag.

uniform concentration distribution was found on the catalyst layers.

The velocity profile at the bottom of the backing layer shows the reason why the serpentine type shows a relatively uniform fuel concentration. Fig. 12 shows the velocity distributions at the bottom of the backing layer of the serpentine and the parallel type flow channel. The velocity of parallel type is of the order of 10^{-7} m s^{-1} which means the convective velocity is nearly

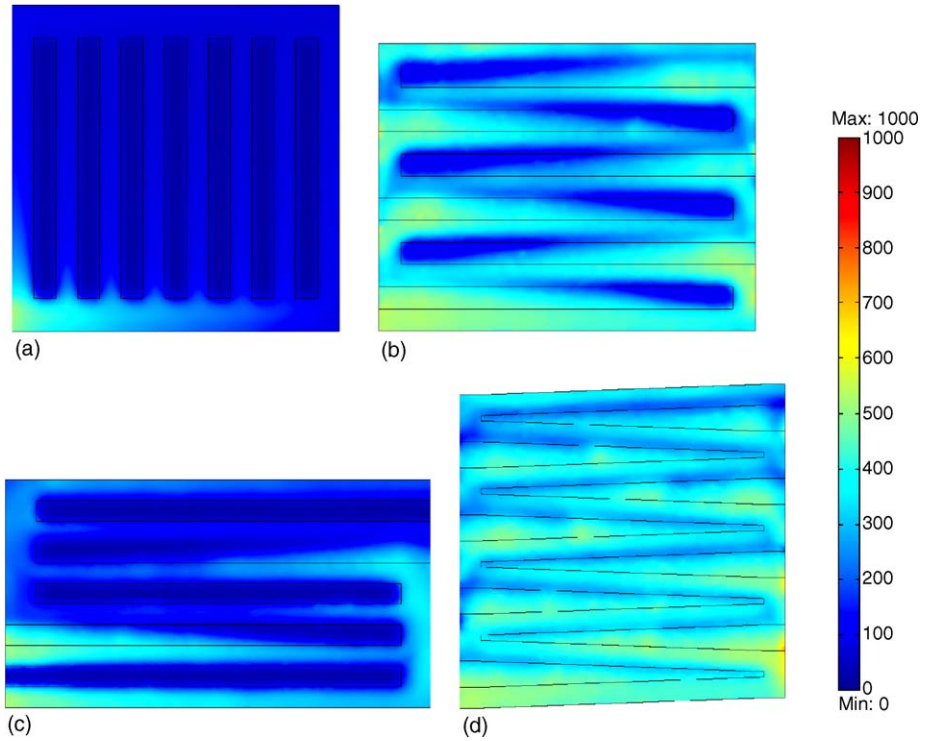

Fig. 8. Concentration distributions at the electrode surface when the overpotential of 0.45 V is imposed. Average concentrations on the catalyst layer: (a) 84 mol m^{-3} for parallel, (b) 303 mol m^{-3} for serpentine, (c) 166 mol m^{-3} for parallel serpentine and (d) 363 mol m^{-3} for zigzag.

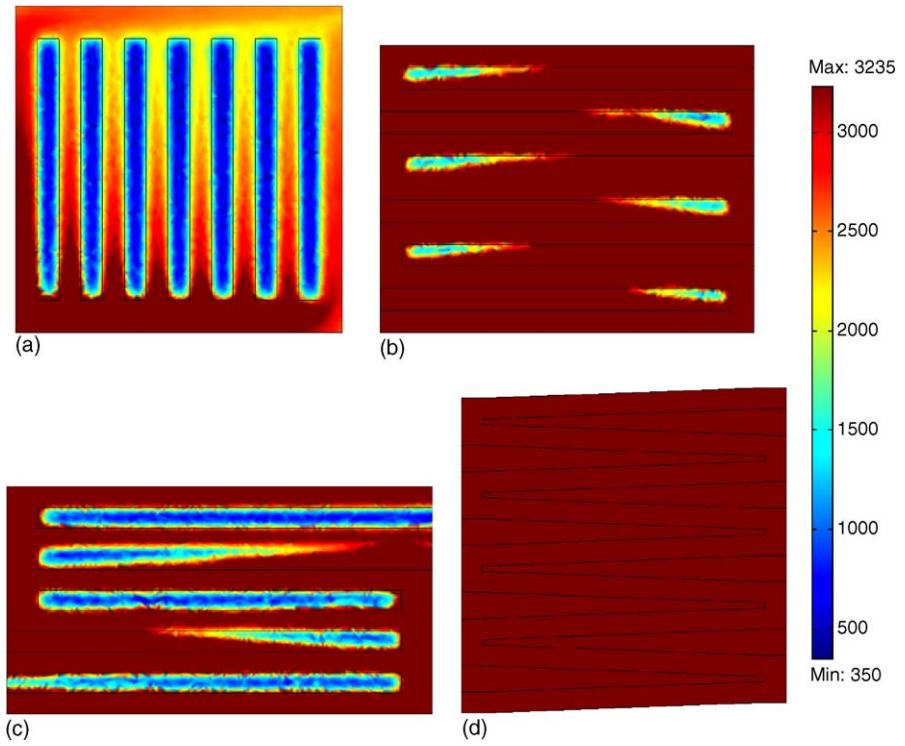

Fig. 9. Current distributions at the electrode surface when the overpotential of 0.45 V is imposed. Average current densities on the catalyst layer: (a) 2087 A m^{-2} for parallel, (b) 3152 A m^{-2} for serpentine, (c) 2723 A m^{-2} for parallel serpentine and (d) 3235 A m^{-2} for zigzag.

negligible and therefore the diffusion through the backing layer is mainly controlled by the mass transfer in the backing layer. However, in serpentine type the velocity at the bottom of the backing layer is 10^3 or 10^4 times higher than that in the parallel type. It means that both convection and diffusion control the mass transfer in serpentine type. The convective velocity is originated from the pressure gradient of the flow fields and makes the mass transfer of fuel easy. Therefore, the velocity from the

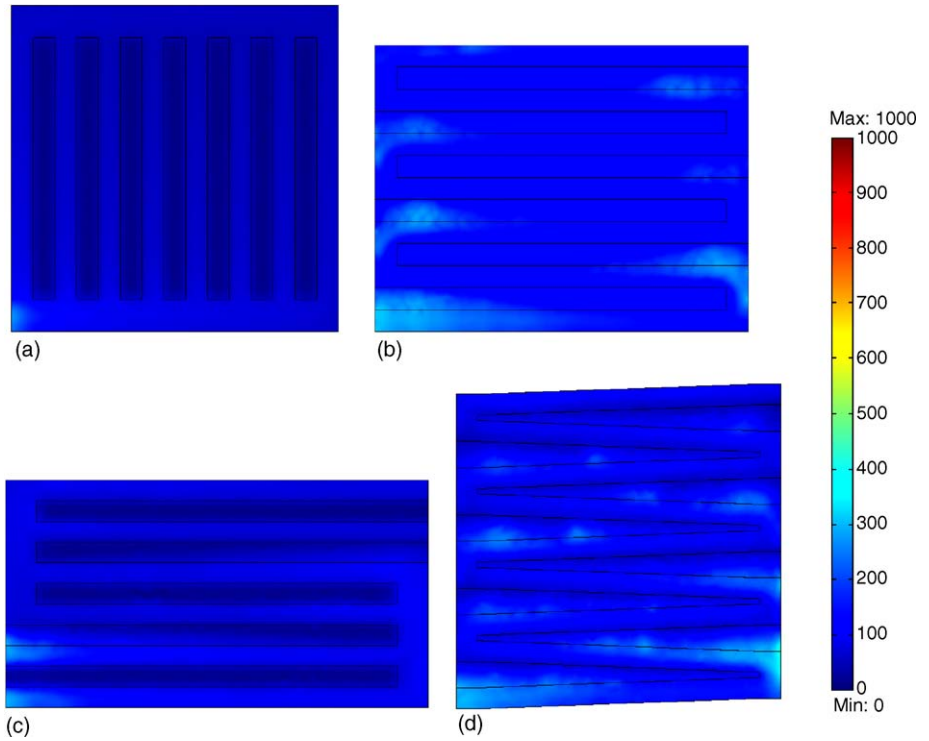

Fig. 10. Concentration distributions at the electrode surface when the overpotential of 0.5 V is imposed. Average concentrations on the catalyst layer: (a) 47 mol m^{-3} for parallel, (b) 107 mol m^{-3} for serpentine, (c) 66 mol m^{-3} for parallel serpentine and (d) 119 mol m^{-3} for zigzag.

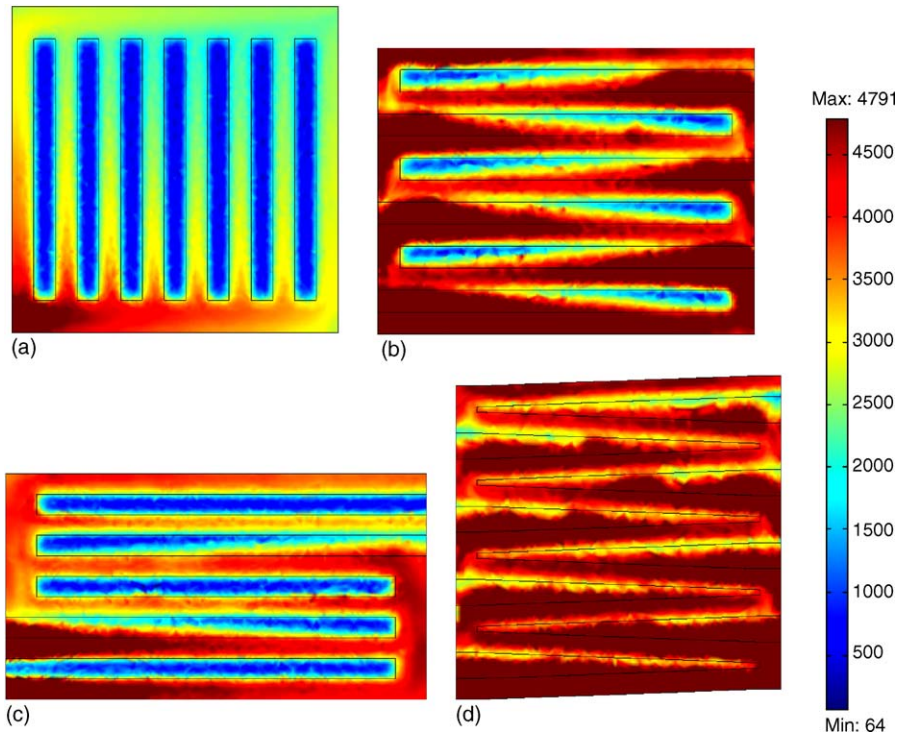

Fig. 11. Current distributions at the electrode surface when the overpotential of 0.5 V is imposed. Average current densities on the catalyst layer: (a) 2186 A m^{-2} for parallel, (b) 3891 A m^{-2} for serpentine, (c) 3003 A m^{-2} for parallel serpentine and (d) 4283 A m^{-2} for zigzag.

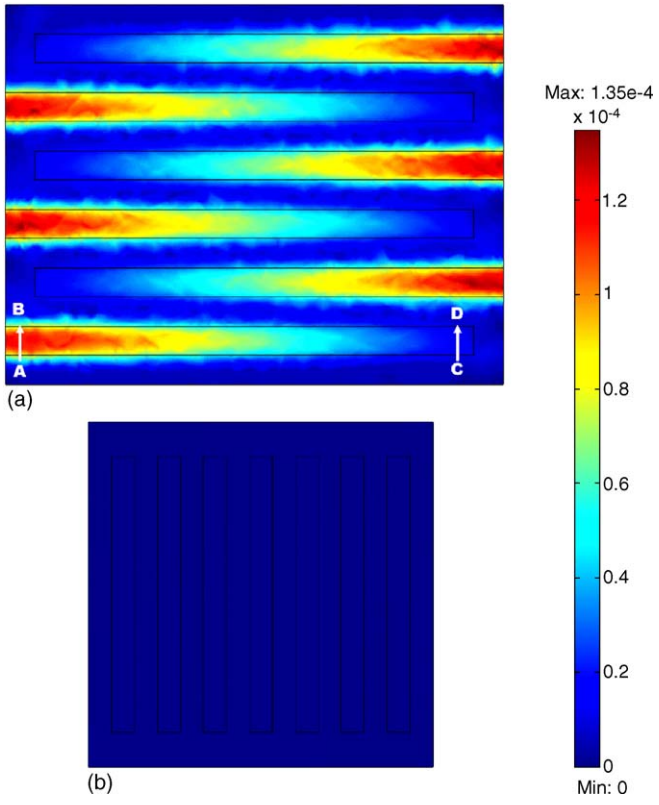

Fig. 12. Velocity profile at the bottom of the backing layer: (a) serpentine and (b) parallel (unit: m s^{-1}).

position A to the position B in Fig. 12(a) is bigger than that from the position C to the position D in Fig. 12(a). Zigzag type compensates this kind of the velocity difference. Finally high pressure drop contributes the formation of uniform concentration. The parallel type does not need high pressure drop in the channel however the serpentine and the zigzag type require the high pressure drop. The pressure difference between the parallel and the serpentine types reaches about 10^2 times (Fig. 13).

The parallel serpentine type is an intermediate type between the serpentine and the parallel. The channel shape of the parallel serpentine is meandering which is similar to serpentine type and the parallel channel of the parallel serpentine is similar to the parallel type. The zigzag type is based on the serpentine type. The main idea of the zigzag type is to make the width from C to D close because the fuel concentration near the bended point of channel is low.

Fig. 14 presents an anode overpotential curve according to the flow-field design. Each point is originated from the average current densities calculated from the methanol concentration at the catalyst layer when the corresponding overpotential is imposed. Dot line is a theoretical activation polarization curve in which the concentration polarization is not considered. According to the simulated results, all types of the flow fields agree the theoretical values well until the overpotential of 0.35 V whereas they cannot overcome the concentration polarization and finally bring out the sudden increment of overpotential. The overpotential curves of the parallel, the parallel serpentine, the serpentine and the zigzag types deviate the theoretical overpotential curve from 142 mA cm^{-2} at 0.35 V, 208 mA cm^{-2} at 0.4 V, 315 mA cm^{-2} at

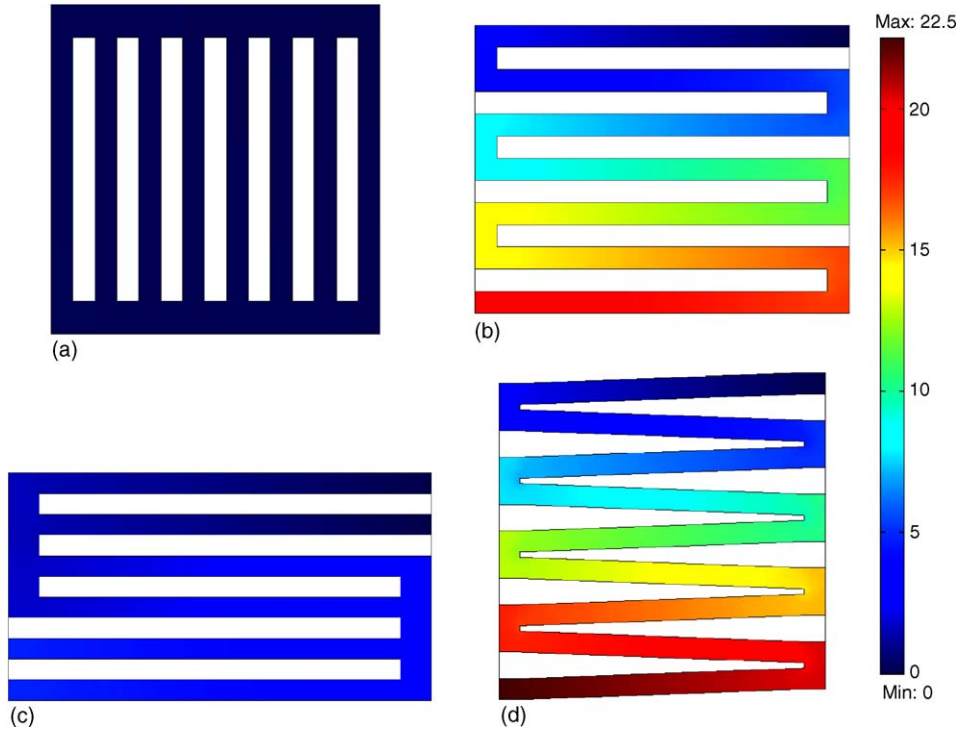

Fig. 13. Pressure drop in the flow-field channel when the fuel input velocity is 1.5×10^{-8} m^3 s^{-1}: (a) 0.18 Pa for parallel, (b) 19.70 Pa for serpentine, (c) 4.95 Pa for parallel serpentine and (d) 22.50 Pa for zigzag.

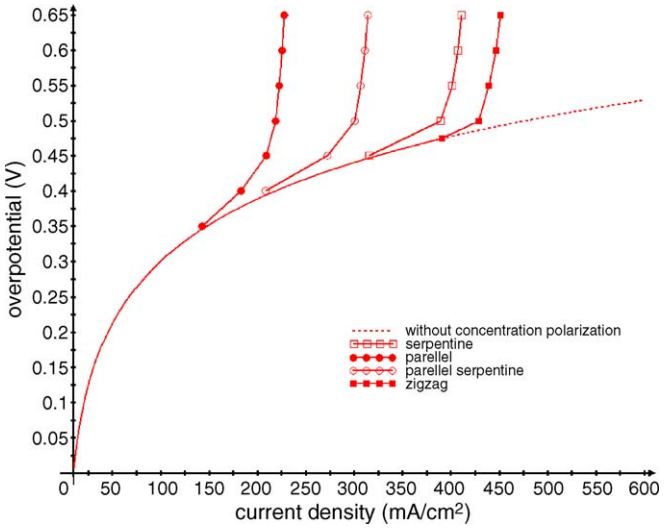

Fig. 14. Predicted anode overpotential curve according to the flow-field design.

0.45 V and 391 mA cm^{-2} at 0.475 V, respectively. Zigzag type can be estimated as the best flow-field shape in this work.

4. Conclusions

A three-dimensional computational simulation of DMFC anode was developed for the parallel, the serpentine, the parallel serpentine and the zigzag types in order to illustrate the performance difference according to the flow-field design. By examining the methanol concentration distribution and the current density distribution the performance of the anode for each flow field was estimated. The zigzag type showed the best performance which has a good resistance against the fuel concentration polarization and the next are the serpentine, the parallel serpentine and the parallel in order. The cell performance was proportional to the pressure drop for all the flow-field types. Pressure energy which forces liquid fuel out of the channels helps fuel to spread uniformly by driving the convective velocity in the backing layer. In this work zigzag type showed the best anode performance whereas needed the highest pressure drop.

Acknowledgement

This work was supported by the Core Technology Development Program for Fuel Cell of Ministry of Commerce, Industry and Energy (MOCIE).

References

[1] J. Larminie, A. Dicks, Fuel Cell System Explained, second ed., Wiley, Chichester, 2003, p. 141.
[2] B.-D. Lee, D.-H. Jung, Y.-H. Ko, J. Power Sources 131 (2004) 207–212.
[3] K. Scott, W.M. Taama, P. Argyropoulos, K. Sundmacher, J. Power Sources 83 (1999) 204–216.
[4] X. Ren, T.E. Springer, T.A. Zawodzinski, S. Gottesfeld, J. Electrochem. Soc. 147 (2) (2000) 466–474.
[5] V. Tricoli, N. Carretta, M. Bartolozzi, J. Electrochem. Soc. 147 (4) (2000) 1286–1290.
[6] D.-H. Jung, Y.-B. Myoung, S.-Y. Cho, D.-R. Shin, D.-H. Peck, Int. J. Hydrogen Energy 26 (2001) 1263–1269.
[7] B. Gurau, E.S. Smotkin, J. Power Sources 112 (2002) 339–352.
[8] Z. Qi, A. Kaufman, J. Power Sources 110 (2002) 177–185.
[9] P. Argyropoulos, K. Scott, W.M. Taama, Electrochim. Acta 44 (1999) 3575–3584.

[10] T. Bewer, T. Beckmann, H. Dohle, J. Mergel, D. Stolten, J. Power Sources 125 (2004) 1–9.
[11] A.A. Kulikovsky, Electrochem. Commun. 7 (2005) 237–243.
[12] H. Yang, T.S. Zhao, Q. Ye, J. Power Sources 139 (2005) 79–90.
[13] A.A. Kulikovsky, J. Appl. Electrochem. 30 (2000) 1005–1014.
[14] Z.H. Wang, C.Y. Wang, J. Electrochem. Soc. 150 (2003) A508–A519.
[15] K. Scott, P. Argyropoulos, J. Power Sources 137 (2004) 228–238.
[16] H. Dohle, K. Wippermann, J. Power Sources 135 (2004) 152–164.
[17] A.S. Arico, P. Cret, V. Baglio, E. Modica, V. Antonucci, J. Power Sources 91 (2000) 202–209.
[18] K. Tüber, A. Oedegaard, M. Hermann, C. Hebling, J. Power Sources 131 (2004) 175–181.
[19] K.Z. Yao, K. Karan, K.B. McAuley, P. Oosthuizen, B. Peppley, T. Xie, Fuel Cells 1–2 (2004) 3–29.